EPJ manuscript No.
(will be inserted by the editor)

Thermal depinning of fluxons in ratchet discrete Josephson rings

Fernando Naranjo[1], Kenneth Segall[2], and Juan J. Mazo[3,4]

[1] Universidad Pedagógica y Tecnológica de Colombia, Tunja, Colombia
[2] Department of Physics and Astronomy, Colgate University, Hamilton NY 13346
[3] Dpto. de Física de la Materia Condensada, Universidad de Zaragoza, 50009 Zaragoza, Spain
[4] Instituto de Ciencia de Materiales de Aragón, C.S.I.C.-Universidad de Zaragoza, 50009 Zaragoza, Spain

the date of receipt and acceptance should be inserted later

Abstract. We study numerically the thermal depinning of single fluxons in ratchet Josephson junction rings. Rings are made of 9 junctions with 3 different critical currents. We present results for a wide range of the main physical parameters of the system: damping, coupling and temperature. The computed results can be well understood in the framework of single particle thermal activation theories.

1 Introduction

A soliton is a spatially localized wave that maintains its shape when it travels, and shows extraordinary stability properties. First studied almost two centuries ago, they have been the object of intense research in the last fifty years since they appear in many dispersive nonlinear systems, in fields so different as fluid dynamics, superconducting circuits, nonlinear electrical circuits, optical fibers, plasma physics, dislocations in crystals, magnetic and ferroelectric domain walls, biomolecule dynamics or Bose-Einstein condensates to mention a few of them [1,2].

One of the three classical equations for studying solitons is the sine-Gordon equation [3]. This equation is the prototype example for the study of topological solitons in 1d, whose distinctive property is its existence not only as dynamical objects but also as static equilibrium solutions of the system. Within the physical systems bearing topological solitons, Josephson-junction superconducting circuits stand out due to their experimental accessibility and technological importance. In these systems, the soliton is frequently referred as fluxon or Josephson vortex since a soliton corresponds to one quantum of flux trapped in the system [4]. Being a long Josephson junction the physical realization of the sine-Gordon equation, a parallel array with short Josephson junctions implements its discrete counterpart: the discrete sine-Gordon equation, also know as Frenkel-Kontorova model [5].

In regular Josephson junction (JJ) parallel arrays, fluxons exhibit marked particle-like properties [6–9] and experiences a symmetric almost sinusoidal pinning potential (the Peierls-Nabarro potential). However, it has been shown [10] that arrays can be configured using suitable combinations of junctions area and cells size to form other potentials, in particular asymmetric periodic ones (the so-called ratchet potentials).

A *ratchet* refers to a device that allows for directional motion under zero mean external forces [11,12], thus showing rectification of zero mean non-equilibrium fluctuations. This phenomenon has been identified in multiple systems including suitable designed superconducting circuits [13–18]. Some of these experiments report the directional motion of solitons in continuous systems, a topic first studied theoretically almost 20 years ago [19].

In this manuscript we numerically characterize some key properties of the dynamics of fluxons in ratchet JJ rings (a circular array with JJ connected in parallel). We will study the current-voltage (IV) characteristics of the system and the thermal depinning of fluxons in asymmetric JJ arrays in a wide range of values of the parameters of the system.

2 The ratchet JJ ring

A JJ is a solid state device made of two superconducting electrodes separated by a thin non-superconducting barrier. Its main physical properties are given by the Josephson relations:

$$V = \frac{\Phi_0}{2\pi}\dot{\varphi}\ , \quad I = I_c \sin\varphi\ ; \tag{1}$$

where φ is the superconducting phase difference in the junction, V and I voltage and current through the junction; I_c the junction critical current (the maximum superconducting current it supports), and $\Phi_0 = h/2e$ the magnetic flux quantum.

It is possible to build well-characterized JJ arrays of many different sizes and geometries. We will consider now a closed parallel array of JJs with possible different junction area and cell size. In this case, in its simplest approach and neglecting external fields, the energy of the system can

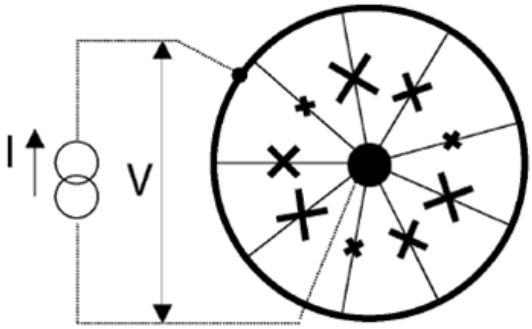

Fig. 1. Sketch of the current biased JJ ratchet ring. Crosses represent JJs of 3 different size.

be written as [7,10]

$$\frac{E}{E_J} = \sum_j h_j(1-\cos\varphi_j) + \frac{\lambda_j}{2}(\varphi_{j+1}-\varphi_j)^2. \qquad (2)$$

Here φ_j is the gauge invariant phase different in every junction of the array and energy is normalized by $E_J = \Phi_0 I_c/2\pi$ with I_c the critical current of one of the junctions, the largest one for instance. The first term to the right of the equal sign accounts for the Josephson energy of the junctions, being $h_j = I_{cj}/I_c$; and the second one for the inductive energy. Here, as usual, we consider only cell self-induced fields and $\lambda_j = \Phi_0/2\pi I_c L_j$ with L_j the self-inductance of cell j.

Two different configurations have been proposed for fluxon ratchet potentials [14]. In the first case the circuit is designed by alternating junctions of two distinct areas (thus two distinct critical currents) and cells of two different sizes (thus two distinct self-inductances). This system was designed, fabricated and measured and thus its ratchet character was verified [14,10]. However, this configuration has an important drawback from the viewpoint of the experimental study of the system: the fact that the cells have different size modifies from cell to cell the magnetic flux induced by the currents in the system and gives more complex magnetic patterns and in a way difficult to control. Therefore, throughout this article we will study a different proposal: an array with junctions of three sizes and identical cells, see Figure 1. In this case λ_j is the same for all cells and we will choose $\{h_j\} = \{1, 0.5, 0.3, 1, ...\}$. Motivated by recent experimental realizations we will present results for a relatively small ring made of 9 JJs.

One of the more notable features of a ratchet array from an experimental point of view is the presence of two depinning currents for the fluxon, depending on the current polarity. Figure 2 shows the two computed depinning currents of the array for different values of the coupling parameter λ. The figure also represents the normalized difference between such currents which shows the existence of a λ value region for which the ratchet character of the array is more pronounced.

For very small values of λ the fluxon effective potential is periodic but the fluxon experiences three different wells per period. Such wells corresponds to the fluxon centered in any of the cells of the array (the corresponding maxima correspond to the fluxon sited on any of the three Josephson junctions). Due to the magnetic induction interaction this potential smooths increasing λ, and at a critical value $\lambda_{c1} \simeq 0.13$ for our junction parameter sequence, one of these maxima and minima vanish through a saddle-node bifurcation. At a larger value coupling, $\lambda_{c2} \simeq 0.23$ a new saddle-node bifurcation happens. For higher values of λ the periodic potential is a ratchet potential with a single well and extends over three cells of the array.

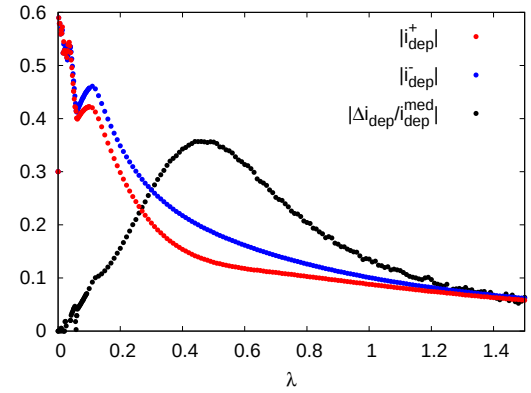

Fig. 2. Depinning currents $|i_{dep}|$ for the fluxon as function of the coupling λ for the ratchet array. We also measure the ratchet character of the array by evaluating $\Delta i_{dep}/i^{med}_{dep}$, the ratio between the difference and the mean value of the absolute values of the two depinning currents, a way of quantifying the magnitude of the asymmetric nature of the array.

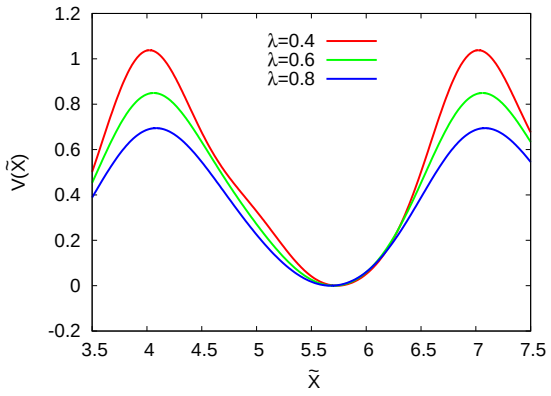

Fig. 3. Peierls-Nabarro potential for the fluxon in a 9 junctions Josephson ratchet ring with $\{h_j\} = \{1.0, 0.5, 0.3, ...\}$ and for λ =0.4, 0.6 and 0.8.

Figure 3 shows the Peierls-Nabarro potential for the fluxon at three values of λ. In all three cases is drawn $V(\widetilde{X}) - V_{min}$, which represents, the energy difference between the maximum and the minimum of the defined Peierls-Nabarro potential. $\widetilde{X}$ is the position of the fluxon center of mass in the array being $\widetilde{X} = 1$ the separation between junctions and $\widetilde{X} = 3$ the potential period. Not only the fluxon potential profile but other relevant physical properties can be computed (see Appendix).

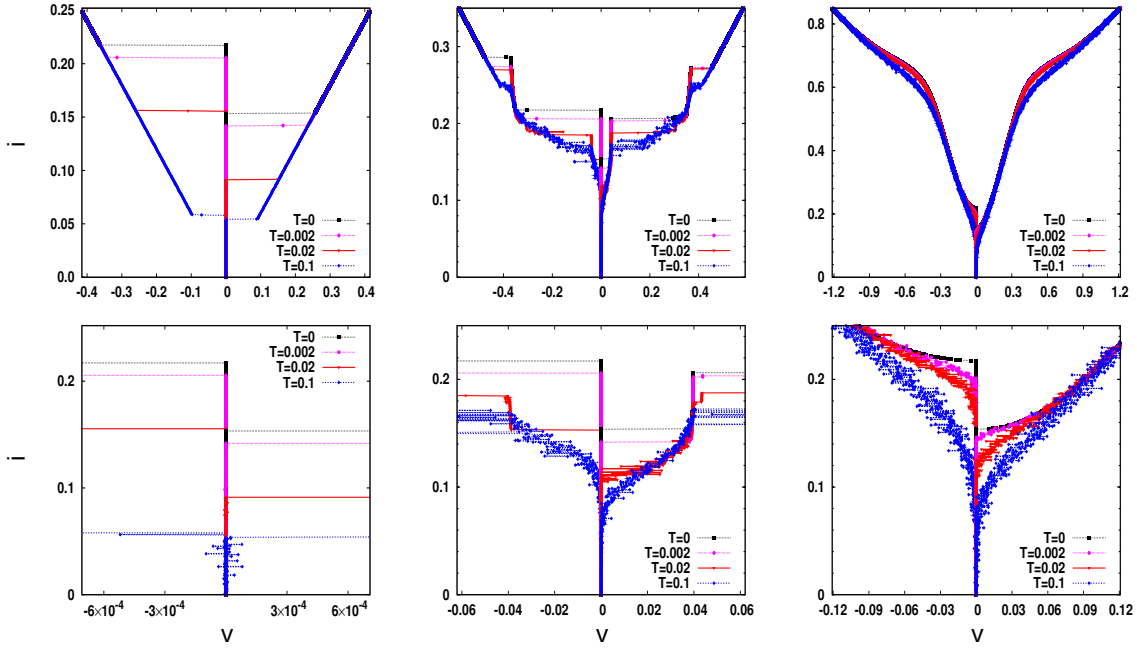

Fig. 4. $|i|$-v for one fluxon in a ratchet ring of 9 junctions at $\lambda = 0.4$. We present curves for three values of damping: $\Gamma = 0.01$ (left), $\Gamma = 0.1$ (center) and $\Gamma = 1.0$ (right). Each plot shows 4 different temperatures (T =0, 0.002, 0.02 and 0.1). Bottom panels are a zoom of the upper ones showing in detail the low voltage region of the curves.

Using lithographic techniques, it is possible to build well characterized Josephson junction arrays. As said, we consider a closed array forming a ring with JJ of three alternating different sizes connected in parallel and forming cells of equal size. The typical experiment with such devices, consists on biasing the array with a dc current and measuring the dc voltage between both electrodes of the ring to know the array critical current and the corresponding IV curves. In order to trap a certain number of fluxons in the ring, a field cooling process is applied prior to electrical measurements. Once cooled, this external field can be removed (or biased at will) but a conserved number of fluxons keep trapped in the array. We will present results for zero final external field.

The system of equations that describes the dynamics of the array, in its simplest approach, can be written as:

$$h_j(\ddot{\varphi}_j + \Gamma\dot{\varphi}_j + \sin\varphi_j) = \lambda(\varphi_{j+1} - 2\varphi_j + \varphi_{j-1}) + i + \tilde{i}_j(\tau) \quad (3)$$

where $j = 1, ...N$ and φ_j is the phase difference across junction j. We take as reference the parameters (I_c, R, C) of the largest junctions and normalize current by the highest critical current, $i = I/I_c$ and $h_j = I_{cj}/I_c$; and time by the plasma frequency $\omega_p = \sqrt{2\pi I_c/\Phi_0 C}$ ($\Phi_0 = h/2e$ is the magnetic flux quantum). The parameter $\Gamma = \sqrt{\Phi_0/2\pi I_c C R^2}$ measures the degree of damping in the system, and the last term in equation $\tilde{i}_j(\tau)$ describes the effect of thermal noise on the dynamics and satisfies $\langle\tilde{i}_j(\tau)\rangle = 0$ and $\langle\tilde{i}_j(\tau)\tilde{i}_k(\tau')\rangle = 2h_j\Gamma T\delta_{jk}\delta(\tau - \tau')$ where we use T for the normalized temperature $T = k_B T_{\rm exp}/E_J$ ($T_{\rm exp}$ is the experimental temperature). The coupling between the junctions is given by the parameter $\lambda = \Phi_0/(2\pi L I_c)$. The normalized voltage v showed by the system is $v = V_{dc}/I_c R = (\Phi_0/2\pi I_c R)\langle d\varphi/dt\rangle = \Gamma\langle d\varphi/d\tau\rangle$. We remark that the boundary conditions are defined by the topology of the array. Here we have considered circular arrangements so that $\varphi_{j+N} = \varphi_j + 2\pi M$ where M the number of fluxons trapped in the system is a constant of the motion. Thus the equations of motion take the form of a system of stochastic differential equations. We have solved them numerically using a Runge-Kutta method.

In the following we consider the case of 1 fluxon, for a network size of 9 junctions with $\{h_j\} = \{1.0, 0.5, 0.3, 1.0, 0.5, 0.3, 1.0, 0.5, 0.3\}$ and $\lambda > 0.25$, to ensure that the fluxon experiences an asymmetric periodic potential similar to those showed in Fig. 3

3 Results

3.1 I-V curves

We will start showing examples of typical IV curves at different parameter values (damping and temperature). Curves were computed for both current polarities but in order to better present the results we plot the obtained voltage v as a function of the current absolute value $|i|$. We follow usual convention in JJ literature of showing voltage in the x-axis of the plot. Voltage was computed at steps of defined current increased from zero with an average ramp of $\frac{8}{3} \times 10^{-7}$ in normalized units. The inductive coupling parameter λ was fixed to 0.4, a value of large asymmetry in the system (see Fig. 2). Three values of damping: low ($\Gamma = 0.01$), moderate ($\Gamma = 0.1$) and high ($\Gamma = 1$) were se-

lected, corresponding to three different physical regimes. The IV curves are shown in Fig. 4.

At this value of λ, the zero temperature depinning currents of the fluxon are approximately $i^{+}_{dep} = 0.154$ and $i^{-}_{dep} = -0.217$. For low damping, at these currents the whole array switches at the ohmic branch where $v \propto i$. Increasing T the fluxon depinning current diminishes by thermal activation over the system pinning barrier. We will study this in more detail below.

A qualitatively different IV is observed for moderate damping values. Two important features of the dynamics of the system can be observed now. At low T, at the depinning current the junction switches first to a resonant state characterized by an step in IV curve. In this state fluxon velocity couples to the electromagnetic linear waves of the ring. Increasing current this state destabilizes and array switches into a new step or into the ohmic branch. An interesting phenomena, already observed in regular arrays [20,21], appears increasing T: the emergence of a thermally activated fluxon diffusion branch where the voltage continuously increases from zero at the depinning. This branch also destabilizes for a given maximum voltage where the system switches to resonant states or to the ohmic branch.

For higher damping no switching is observed and voltage increases continuously from zero at the depinning current. For low current values the fluxon travels around the ring maintaining its localized character. At higher currents fluxon delocalizes and a clear change in the curve slope is observed. In this case temperature causes a decreasing of the depinning current and a rounding of the IV curve at low voltages.

All curves show an asymmetry at low voltages and in all the cases it is also observed that as the temperature increases the asymmetry of the IV curve reduces. This is easy to understand since at high temperatures the details of the potential are screened by the intensity of thermal fluctuations.

Simulations performed at other values of λ in the ratchet region of the device reveal the same physical scenario that the one described above.

3.2 $\langle i_{\rm dep}(T)\rangle$

Overdamped arrays can be designed shunting every junction with a small resistance. However, unshunted junctions usually have Γ values in the moderate and low damping range and show a well defined switching current. Thus, we will study now the thermal change of both, the positive and negative, switching currents of our ratchet arrays for two small values of damping (Γ =0.001 and Γ =0.01) and three values of the coupling $\lambda = 0.4$, $\lambda = 0.6$ and $\lambda = 0.8$. Later, we will interpret the obtained results in a common physical framework.

$\lambda =$	$i^{+}_{dep}(T=0)$	$i^{-}_{dep}(T=0)$	Δi_{dep}	$\Delta i_{dep}/i^{med}_{dep}$
0.4	0.154	-0.217	0.063	0.34
0.6	0.118	-0.162	0.044	0.31
0.8	0.103	-0.127	0.024	0.21

Table 1. Quantitative estimation of the asymmetry in the depinning of a fluxon in a ratchet network for $T = 0$. $\Delta i_{dep} = |i^{+}_{dep} + i^{-}_{dep}|$ and $i^{med}_{dep} = \frac{1}{2}(|i^{+}_{dep}| + |i^{-}_{dep}|)$.

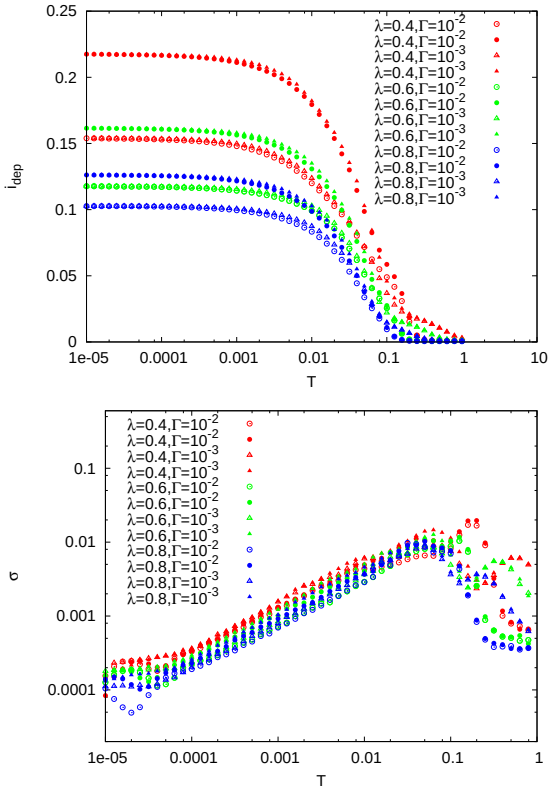

Fig. 5. Top Figure: Mean value of the depinning current of a fluxon in a ratchet network with 9 junctions for $\lambda = 0.4$ (red), $\lambda = 0.6$ (green) and $\lambda = 0.8$ (blue). Curves for two values of the damping, $\Gamma = 0.01$ (circles) and $\Gamma = 0.001$ (triangles), are shown. Both depinning currents: i^{+}_{dep} (open symbols) and $|i^{-}_{dep}|$ (filled symbols), are plotted. The averages have been performed over 1000 realizations. Bottom figure shows the value of the standard deviation σ results.

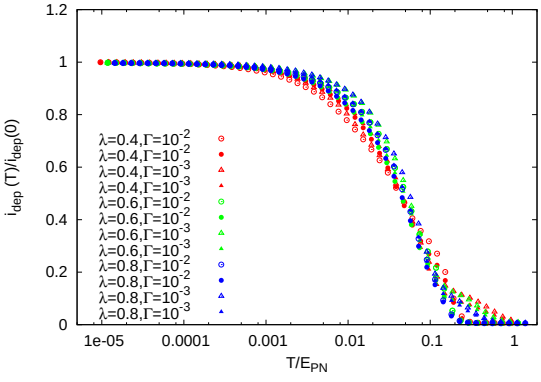

Fig. 6. Normalized depinning current versus temperature curves.

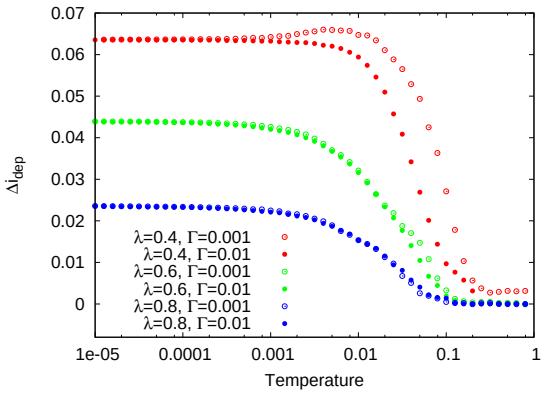

Fig. 7. The figure shows the value of Δi_{dep} defined as $\Delta i_{dep} = |i^-_{dep}| - |i^+_{dep}|$ as a function of the temperature for different values of λ and Γ.

Figures 5 show the results of the simulations. Each point comes after averaging 1000 realizations and the mean value of the switching current and the standard deviation are plotted. As temperature increases the array switches at a smaller value of current. As shown in the figure the decreasing is more evident for $T > 0.001$, where temperature is high enough to cause an observable switching by thermal activation. All curves show a similar behavior with small differences between the two chosen damping values. For $T \sim 0.1$ thermal fluctuations are large enough to switch the system even at very low currents.

We can try to understand within a common framework the set of results presented in Figure 5. This can be achieved if current is normalized in every curve by the zero temperature depinning current and temperature by the zero current PN barrier (see tables). Results are shown in Fig. 6. Overlapping is excellent for all the curves.

To finish, in Fig. 7 we compare the evolution of the degree of asymmetry of the system. To do this we define $\Delta i_{dep} = |i^-_{dep}| - |i^+_{dep}|$. As can be seen, for $\lambda = 0.6$ and $\lambda = 0.8$ this measure decreases monotonically with temperature and there is no difference between the two values of the studied damping. However, the case $\lambda = 0.4$ and low damping is not as simple as the parameter Δi_{dep} reaches a maximum for $T \sim 0.01$. In addition, for $T > 0.001$, when Δi_{dep} starts to grow up, differences between the cases Γ=0.001 and Γ=0.01 are observed. It is worth noting that the value of such a difference is small when compared to the absolute depinning current values. Thus, this *anomaly* is not detected in the previous plots.

3.3 The fluxon as a single particle picture

Being a spatially localized entity, the fluxon has marked particle-like properties. This issue has been the object of many studies in the past [22,5]. In this section we will follow this perspective and analyze thermal fluxon depinning at the light of the fluxon as a single particle picture theory. We performed a similar analysis in the past for fluxon in regular arrays [20], so we will shorten here the presentation of the theory and show our numerical results.

As previously said, the localized fluxon behaves as a single particle experiencing the periodic (ratchet in this case) potential shown in Fig. 3. Then the theoretical analysis of the fluxon thermal depinning can be done in the framework of the thermal escape problem of a particle in a mestastable potential (see [23,24] for a review of the general theory and [25,26] for recent progress in the subject in different damping regimes). Though different theories are available, we will based our analysis in the Bütikker, Harris and Landauer (BHL) [27] approach to the problem, an orientation that have been successfully used in the past to study the thermal switching of underdamped single Josephson-junctions [28,29]. There, the tilted potential is approached by a cubic one, a case for which simple analytic results for the escape rate are known.

In the framework of this picture the fluxon potential barrier diminishes with the external current i as

$$\Delta U = E_{PN}\left[(1-\hat{i}^2)^{1/2} - \hat{i}\arccos\hat{i}\right] \tag{4}$$

and the oscillation frequency as

$$\omega_a = \omega_{PN}(1-\hat{i}^2)^{1/4} \tag{5}$$

where $\hat{i} = i/i^0_{dep}$, with the appropriate zero temperature depinning current in each case. See also the basic parameter for the theory in Table 2. The remaining important parameter for the theory is the rate of change of the applied current or ramp in the experiment or in the simulation. It is well know that ramp should be slow enough to avoid several nonequilibrium deviations.

	i^+_{dep}	i^-_{dep}	E_{PN}	ω_{PN}	m
λ =0.4	0.154	-0.2177	1.038	1.806	0.22
λ =0.6	0.118	-0.1616	0.8494	1.5461	0.175
λ =0.8	0.103	-0.1265	0.6944	1.402	0.155

Table 2. Characteristic parameters of a fluxon in ratchet network with 9 junctions

Based in these results, we have calculated numerically the BHL prediction for the depinning current of the array with a fluxon and its standard deviation and compare to our simulations (Fig. 8). We can see that the theoretical predictions agree reasonably well with the performed simulations specially for larger λ values. As expected also BHL theory results are worse for lower damping values where predicted rates deviates from real ones [25].

4 Discussion and Conclusions

We have characterized the thermal depinning of single fluxons in JJ ratchet arrays. The array consists of 9 junctions connected in parallel, forming a ring geometry and alternating junctions of 3 different sizes, assuring periodic fluxon asymmetrical potentials which spread over three

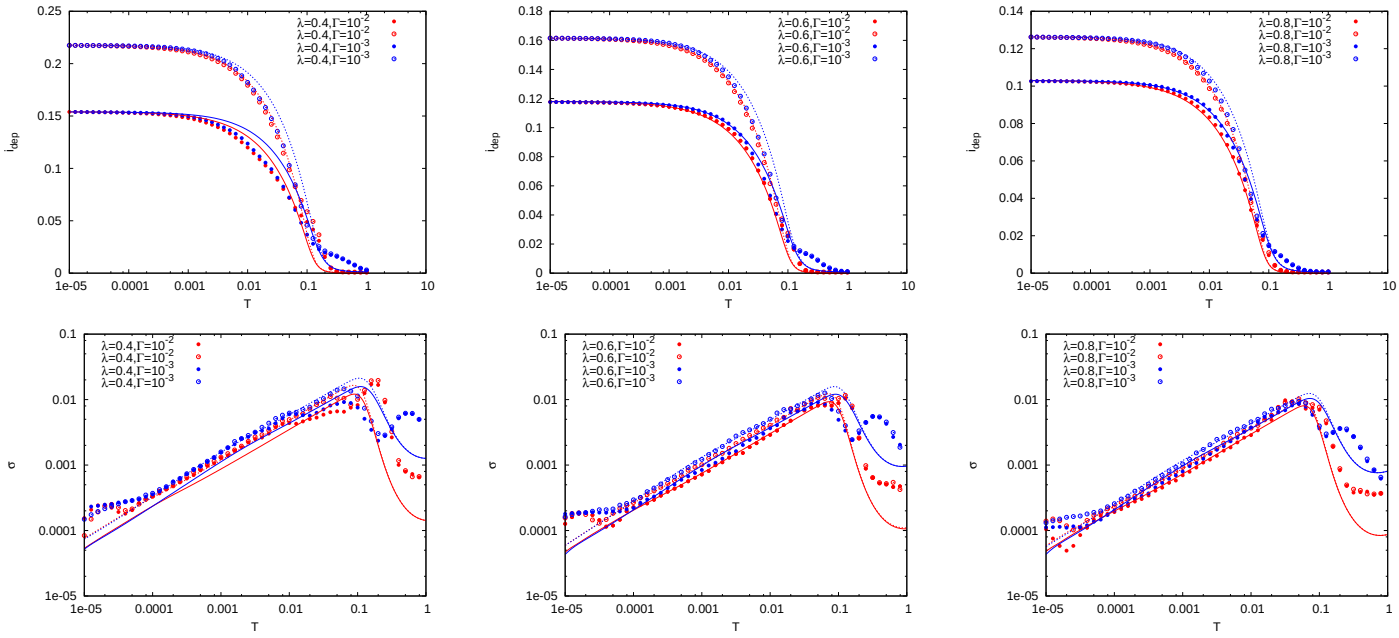

Fig. 8. Comparison of the results obtained for the positive (solid symbols) and negative (open symbols) depinning current at different T of a fluxon in the ratchet array with $\lambda = 0.4$ (left), $\lambda = 0.6$ (center) and $\lambda = 0.8$ (right) to the predictions of the theory BHL escape of a particle in a metastable potential. In each figure results for two values of damping are shown.

cells of the network with a single well every potential period. The results show the asymmetry in the definition of the depinning currents and curves I-V. We have carefully studied the behavior of the depinning currents at low damping and proved that the obtained curves can be understood within a common framework and are reasonably well approximated by the thermal activation theory of single particles.

The difference between the escape currents in both directions of the ratchet is relatively constant with the variation of damping. Such magnitude which somehow measures the asymmetry of the systems shows a maximum for $\lambda \sim 0.5$. This work helps to design future experiments and paves the way to study the behavior of fluxons in quantum regular and ratchet Josephson arrays which can be achieved using smaller junctions and lower temperatures.

JJM acknowledges support from the Spanish MINECO, Project No. FIS2011-25167, cofinanced by FEDER funds, and Gobierno de Aragón (FENOL group). FNM is supported by DIN-UPTC, Colombia. KS acknowledges support from NSF, DMR 1105444.

Appendix: Fluxon characterization

In this manuscript we have studied different dynamical properties of a fluxon in a ratchet array with an emphasis in its particle-like behavior. Now we will describe this analogy in more detail. In order to do this, first we have to introduce the new collective variable X defining the *position* of the fluxon in the array $X = C \mp \sum_j \varphi_j$ (sign stands for fluxon or anti-fluxon configurations respectively). Then, in its simplest approximation, the dynamics of the fluxon in the ring, described by Eq. 3, can be reduced to the dynamics of a massive forced and damped stochastic particle experiencing a substrate PN potential $V(X)$:

$$m\ddot{X} + m\eta\dot{X} + V'(X) = F + \xi(\tau) \qquad (6)$$

The origin of the potential is the discrete character of the array; m states for the kink effective mass (in principle a position dependent quantity $m(X)$ as shown in Fig. 10 as a product of the fluxon elasticity, whose shape changes when moving along the array); the effective biasing force $F = i$, as result of power input comparison; and $\eta \simeq \Gamma$ in the simplest approach.

In Fig. 3 we showed the computed fluxon Peierls-Nabarro potential of the system (we define $\tilde{X} = X/2\pi$). Figure 9 shows the variation of three fluxon parameters as a function of the inductive coupling parameter λ: the Peierls-Nabarro barrier, the asymmetry and the PN frequency or the frequency of the fluxon oscillations around its equilibrium position at the bottom of the potential well. The PN barrier is a key concept in the theory and controls the thermal activation escape of the fluxon. We can see that for large (λ), when array asymmetry is negligible, $i_{dep} \simeq E_{PN}/6$ (prediction for a period 3 sinusoidal potential) but this prediction fails in the asymmetric potential parameter region.

An approximate measure of the asymmetry of the network is to compute the deviation of the difference between the maximum and minimum position. Thus in the case of a regular network of period 3, this difference should be equal to 1.5. Figure 9 shows the calculation of the position of the minimum and maximum of the potential and

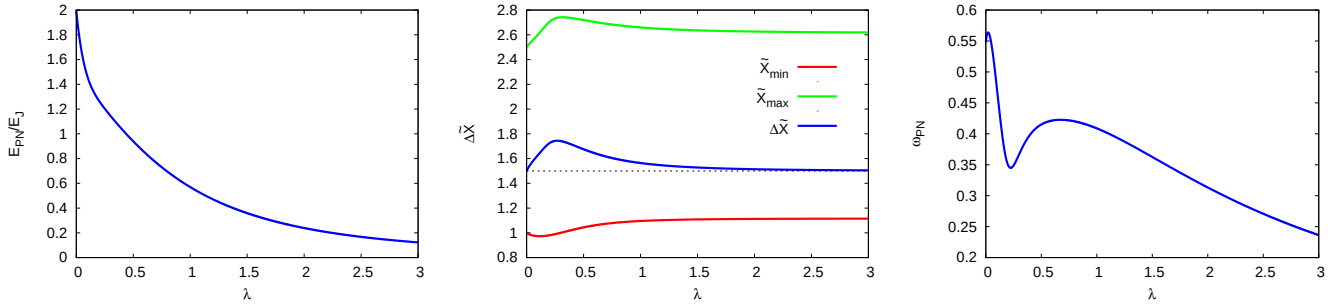

Fig. 9. Fluxon parameters at different λ values for a $h_j = \{1.0, 0.5, 0.3, ...\}$ Josephson ring. Left: Peierls-Nabarro barrier. Middle: $\Delta(\widetilde{X}) = \widetilde{X}_{max} - \widetilde{X}_{min}$, which measures the asymmetry of the network. Right: Peierls-Nabarro frequency $\omega_{PN}(\lambda)$.

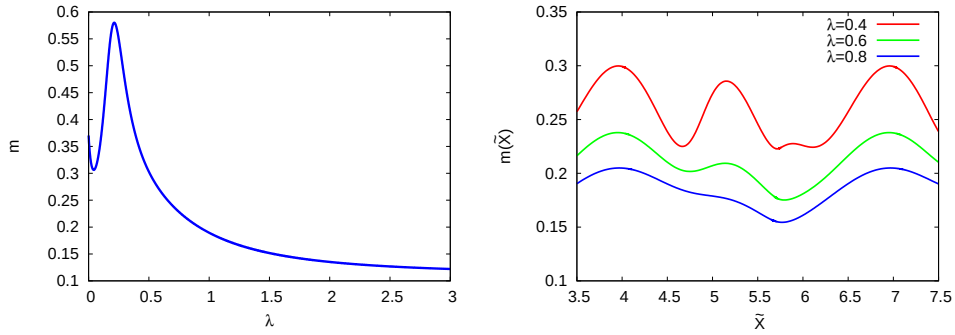

Fig. 10. Left: Estimation of the effective mass of the rest fluxon at the bottom of the potential well. Right: Position dependence of the fluxon effective mass $m(\widetilde{X})$ at λ =0.4, 0.6, 0.8.

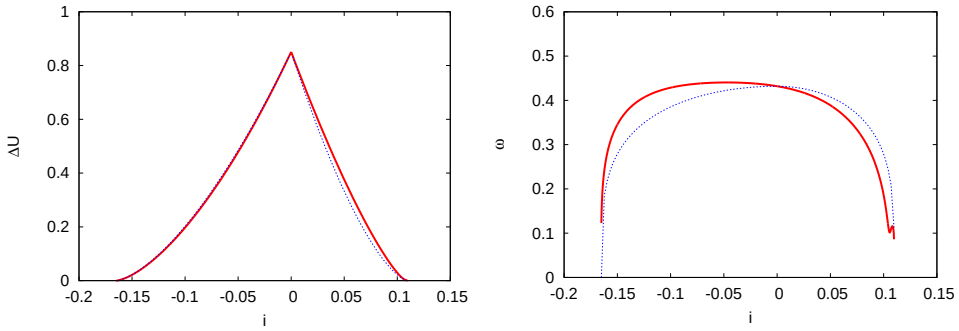

Fig. 11. Peierls-Nabarro barrier and frequency for different values of the external current i at λ =0.6.

the difference between the two values. It can be seen that the asymmetry is more pronounced for values of $\lambda \simeq 0.4$. which is an optimal to select for the study of the network.

Regarding the PN frequency, we observe a complex non-monotonic behavior. This behavior is also observed as expected in the computation of the coupling dependence of the effective mass of the system (Fig. 10). Mass, PN barrier and PN frequency where computed independently and approximately satisfies the expected relation $m \simeq E_{PN}/(2 \times 9\omega_{PN}^2)$. Figure also shows the mass as function of the position of the center of mass of fluxon, $m(X)$ at $\lambda = 0.4$, 0.6 and 0.8. We can see the complexity of the dependence on the existence of several local minima and maxima at small values of λ and the gradual disappearance with increasing the value of the coupling constant of the network.

To finish, in order to understand the fluxon thermal activation process it is important to observe the evolution of potential barrier and frequency as tilted by a positive or negative external current. Figure 11 shows our computed which validates the dependencies assumed in Eq. (4). Regarding the frequency, Eq. (5), the agreement is not so good. However it affects weakly the theoretical results since the escape rate values are dominated by the exponential factor $\Delta U/k_BT$.

References

1. T. Dauxois and M. Peyrard, *Physics of Solitons* (Cambridge University Press, 2006).

2. A. Scott, *Nonlinear Science: Emergence and Dynamics of Coherent Structures* (Oxford University Press, 2003). 2nd edition.
3. J. Cuevas-Maraver, P. G. Kevrekidis, and F. Williams (editors), *The Sine-Gordon Model and its Applications* (Springer, 2014).
4. A. V. Ustinov, Physica D **123**, 315 (1998).
5. O. M. Braun and Y. Kivshar, *The Frenkel-Kontorova Model: Concepts, Methods, and Applications* (Springer, 2004).
6. A. V. Ustinov, M. Cirillo, and B. A. Malomed, Phys. Rev. B **47**, 8357 (1993).
7. S. Watanabe, H. S. J. van der Zant, S. H. Strogatz, and T. P. Orlando, Physica D **97**, 429 (1996).
8. P. J. Martínez, F. Falo, J. J. Mazo, L. M. Floría, and A. Sánchez, Phys. Rev. B **56**, 87 (1997)
9. J. J. Mazo, in *Energy Localization and Transfer: Advanced Series in Nonlinear Dynamics*, edited by A. Litvak-Hinenzon, R. S. Mckay, A. Spanoudaki, and T. Dauxois (World Scientific, Singapore, 2000), pp. 193-246.
10. F. Falo, P. J. Martínez, J. J. Mazo, T. P. Orlando, K. Segall, and E. Trías, Appl. Phys. A **75**, 263 (2002).
11. P. Hänggi, Phys. Rep. **361**, 57 (2002).
12. P. Hänggi and F. Marchesoni, Rev. Mod. Phys. **81**, 387 (2009).
13. I. Zapata, R. Bartussek, F. Sols, and P. Hänggi, Phys. Rev. Lett. **77**, 2292 (1996).
14. E. Trías, J. J. Mazo, F. Falo and T. P. Orlando, Phys. Rev. E **61**, 2257 (2000).
15. G. Carapella and G. Costabile, Phys. Rev. Lett. **87**, 077002 (2001).
16. M. Beck, E. Goldobin, M. Neuhaus, M. Siegel, R. Kleiner, and D. Koelle, Phys. Rev. Lett. **95**, 090603 (2005)
17. A. Sterck, D. Koelle, and R. Kleiner, Phys. Rev. Lett. **103**, 047001 (2009)
18. D. E. Shalom, and H. Pastoriza, Phys. Rev. Lett. **94**, 177001 (2005).
19. F. Marchesoni, Phys. Rev. Lett. **77**, 2364 (1996).
20. J. J. Mazo, F. Naranjo, and K. Segall, Phys. Rev. B **78**, 174510 (2008).
21. K. Segall, A. P. Dioguardi, N. Fernandes, and J. J. Mazo, J. Low Temp. Phys. **154**, 41 (2009)
22. O.M. Braun and Y. S. Kivshar, Phys. Rep. **306**, 1 (1998).
23. P. Hänggi, P. Talkner, and M. Borkovec, Rev. Mod. Phys. **62**, 251 (1990).
24. E. Pollak and P. Talkner, Chaos **15**, 026116 (2005).
25. J. J. Mazo, F. Naranjo, and D. Zueco, Phys. Rev. B **82**, 094505 (2010).
26. J. J. Mazo, O. Y. Fajardo, and D. Zueco, J. Chem. Phys. **138**, 104105 (2013).
27. M. Büttiker, E. P. Harris, and R. Landauer, Phys. Rev. B **28**, 1268 (1983).
28. J. M. Martinis, M. H. Devoret, and J. Clarke, Phys. Rev. B **35**, 4682 (1987).
29. The BHL approach has been shown to apply to short junctions. Alternative theories for long JJ can be found in P. Hänggi et al. Phys. Rev. Lett. **60**, 2563 (1988) and F. Marchesoni, Phys. Rev. Lett. **73**, 2394 (1994).